# Advances into chemometric control of commercial diesel adulteration by kerosene using IR spectroscopy

Heloise O. M. A. Moura[1,#], Anne B. F. Câmara[1], Marfran C. D. Santos[1], Camilo L. M. Morais[2], Leomir A. S. de Lima[1], Kássio M. G. Lima[1], Luciene S. de Carvalho[1,*]

[1] Post-Graduation Program in Chemistry, Federal University of Rio Grande do Norte, 59078-900, Natal, BR.

[2] School of Pharmacy and Biomedical Sciences, University of Central Lancashire, Preston PR1 2HE, UK.

[#]E-mail address: helo.medeiros@outlook.com

[*]E-mail address: luciene_car@hotmail.com

## Abstract

Adulteration is a recurrent issue found in fuel screening. Commercial diesel contamination by kerosene is highly difficult to be detected via physicochemical methods applied in market. Although the contamination may affect diesel quality and storage stability, there is a lack of efficient methodologies for this evaluation. This paper assessed the use of IR spectroscopies (MIR and NIR) coupled with partial least squares (PLS) regression, support vectors machine regression (SVR) and multivariate curve resolution with alternating least squares (MCR-ALS) calibration models for quantifying and identifying the presence of kerosene adulterant in commercial diesel. Moreover, principal component analysis (PCA), successive projections algorithm (SPA) and genetic algorithm (GA) tools coupled to linear discriminant analysis were used to observe the degradation behavior of 60 samples of pure and kerosene-added diesel fuel in different concentrations over 60 days of storage. Physicochemical properties of commercial diesel with 15% kerosene remained within conformity with Brazilian screening specifications; in addition, specified tests were not able to identify changes in the blends' performance over time. By using multivariate classification, the samples of pure and contaminated fuel were accurately classified by aging level into two well-defined groups, and some spectral features related to fuel degradation products were detected. PLS and SVR were accurate to quantify kerosene in the 2.5–40% (v/v) range, reaching RMSEC<2.59% and RMSEP<5.56%, with high correlation between real and predicted concentrations. MCR-ALS with correlation constraint was able to identify and recover the spectral profile of commercial diesel and kerosene adulterant from the IR spectra of contaminated blends.

**Keywords:** Diesel fuel, Adulteration, Kerosene, Multivariate analysis, Storage stability.

## Introduction

An increase in energy and fuel consumption worldwide has encouraged researchers to study new energy sources and look for the best ways to use them. Nowadays, the most important problem faced in the fuel screening field is adulteration, which occurs during the route between the refinery and gas stations to provide illegal profit to scammers [1,2]. In Brazil, gasoline adulteration is currently well controlled in the Fuel Quality Monitoring Program (PMQC) founded by the National Agency of Petroleum, Natural Gas and Biofuels (ANP), using specific analysis of markers added to solvents that can be used as contaminants [3]; however, there is no specific methodology for detecting adulterants in diesel, which is the most consumed fuel in the country [4,5].

Biodiesel, kerosene and vegetable oils are the main adulterants of diesel reported in literature due to its affordability and lower cost in comparison to the original fuel [6]. Biodiesel is a renewable fuel composed of esters that is blended into Brazilian diesel (10% v/v) due to ANP requirements for reducing the emission of harmful gases, but scammers have illegally added a greater amount of biodiesel due to its cheaper production [7]. Kerosene solvent is a cheap petroleum distillate that has similar hydrocarbon composition to diesel and is widely used for adulteration, making it practically impossible to detect this contaminant via physicochemical property tests and other univariate methods [8].

Fuel contamination can cause many problems to burning and storage quality, with the latter being directly associated with the oxidative stability of fuel and signifies how much they resist degradation processes. Diesel and mainly biodiesel components are susceptible to oxidation and hydrolysis reactions over time; thus, the composition of the fuel blend changes over time and the presence of an uncontrolled substance used for adulteration can exert some influence on the process, affecting its quality due to aging [9]. Despite this, ANP specifications do not regulate tests to observe the degradation level of commercial diesel over time due to the lack of a methodology that performs efficient quality screening of this parameter during fuel storage [5]. Therefore, mathematical tools provided by chemometrics enable analyzing multivariate results generated by simple techniques such as infrared (IR) spectroscopy in a way that statistical methods for univariate systems may be inadequate, with accurate, fast and detailed responses [10,11].

Principal component analysis (PCA), successive projections algorithm (SPA) and genetic algorithm (GA) are techniques that promote intelligent experimental data reduction. PCA reduces data to principal components, while SPA and GA reduce it to selected variables. This procedure can improve the potential of the supervised linear

discriminant analysis (LDA) for discriminating the samples in their respective classes due to the lower data complexity. The combinations PCA-LDA, SPA-LDA and GA-LDA are often used in combination for a wide range of applications [12-15], but their potential is not widely explored for screening diesel quality [16].

In case of quantifying kerosene into commercial diesel fuel, the use of a calibration model capable to deal efficiently with non-linear relationships and high dimensional input vectors as support vectors machine regression (SVR) is crucial, since the widely used partial least squares (PLS) has limited performance with complex systems [17]. A promising tool for analyzing fuel adulteration is the multivariate curve resolution with alternating least squares (MCR-ALS). This technique stands out due to its capability to quantify and identify the analyte in the presence of interferences in samples, since these interferences are presented in the calibration samples [18]. In addition, this technique presents some advantages in relation to PLS, such as the smaller number of samples needed and the capacity to quantify and identify interferences (adulterants) in samples without previous knowledge of them, which can be called "second order advantage" [19].

This paper evaluates the efficiency of multivariate tools to solve important issues in diesel screening using NIR and MIR spectroscopies. PLS, SVR and MCR-ALS were applied to quantify and identify the presence of kerosene adulterant in commercial diesel. PCA-LDA, SPA-LDA and GA-LDA models were used to classify and observe the degradation behavior of pure and kerosene-added diesel fuel samples in different concentrations over 60 days of storage. Oxidative stability analysis were performed by PetroOxy accelerated oxidation method to compare with the classification results, in addition to atmospheric distillation, crystallization, specific mass and viscosity tests specified by ANP.

## Materials and Methods

### Sample Preparation

Diesel S10B10 samples with 10% (v/v) of Brazilian commercial biodiesel (soybean oil biodiesel) and 10 mg $kg^{-1}$ sulfur were kindly donated by Clara Camarão Potiguar Refinery (RPCC) and mixed up to different concentrations of commercial kerosene solvent at the Energetic Technology Laboratory (LTEN) for simulating the adulteration process. The samples were divided in two datasets. In the first one, which involves classification models, were used concentrations in the range 5 to 25% (v/v), with increments of 2.5% (v/v) and precision of 0.05%. Each blend was divided into six parts of the same volume and placed in six different amber flasks, making a total of sixty samples.

All flasks were encoded, sealed and stored in a closed box at room temperature for sixty days, along with samples of pure S10B10. Six analysis periods were defined for monitoring physicochemical properties and MIR/NIR features of the mixtures during storage, namely days 0 (beginning of storage), 7, 15, 30, 45 and 60.

For the second dataset, used for adulterant quantification with regression methods such as PLS, SVR and MCR-ALS were produced 16 samples ranging from 2.5 to 40% (v/v). MIR and NIR spectra were recorded for modeling.

**Physicochemical Analysis**

All samples were submitted to MIR and NIR analysis on monitoring days, but only the pure S10B10 and 15% kerosene (Q0 and Q15) samples had some of their physicochemical properties evaluated in order to observe possible changes in composition and properties as a result of the added kerosene and/or storage time. Table 1 shows the reference methods of specified ANP physicochemical analysis, in addition to oxidative stability PetroOXY test, employed for monitoring samples Q0 and Q15 following regulations determined by ASTM International. In addition, some properties inferred for diesel S10B10 and kerosene solvent are depicted.

**Table 1.** Physicochemical analysis and ASTM standards used in this work.

| Analysis | Diesel S10B10 | Commercial kerosene solvent | Standard [20-23] |
|---|---|---|---|
| PetroOXY induction period (IP) (min) | 60.0 | - | ASTM D7545 |
| Atmospheric distillation (°C): | | | |
| 10% distillate | 192.9 | - | ASTM D86 |
| 50% distillate | 281.1 | | |
| Kinematic viscosity at 40 °C ($mm^2/s$) | 3.21 | 2.86 | ASTM D7042 |
| Specific mass at 20 °C ($kg/m^3$) | 828.0 | 786.0 | ASTM D7042 |
| Cloud point (°C) | 0.40 | - | ASTM D2500 |

**Spectral Data Analysis**

MIR measurements were carried out on a Shimadzu IRAffinity-1 spectrometer equipped with an attenuated total reflectance (ATR) sample holder and ZnSe crystal. The results were obtained in a wavenumber range from 700-

4000 $cm^{-1}$ with resolution of 4 $cm^{-1}$ and 32 scans. NIR data were obtained using a spectrometer from ARCoptix with a quartz cuvette of 1.00 mm in transmission mode. The NIR readings were performed using ARCspectro software version 1.6 in a wavelength range from 1000-2500 nm and resolution of 8 nm.

Data pre-treatment and construction of the classification and calibration models were performed using MATLAB R2012b software (MathWorks Inc., Natick, USA) with PLS Toolbox version 7.9.3 (Eigenvector Research, Inc., Manson, USA). For the development of multivariate models, baseline correction, Savitzky-Golay smoothing (window of 15 points) and mean center were performed on the MIR spectra dataset for denoising; whereas the NIR data were pre-processed by using multiplicative scatter correction (MSC), Savitzky-Golay smoothing (window of 15 points) and mean center.

Before modeling, spectral data were divided into training (70%), validation (15%) and prediction (15%) sets for applying LDA to PCA, SPA and GA scores; and calibration (70%) and prediction (30%) sets for PLS regression, by applying the classic Kennard-Stone (KS) uniform sampling selection algorithm [24]. Cross-validation "leave-one-out" was used for PLS. The overall methodology developed in this research is depicted in Scheme 1.

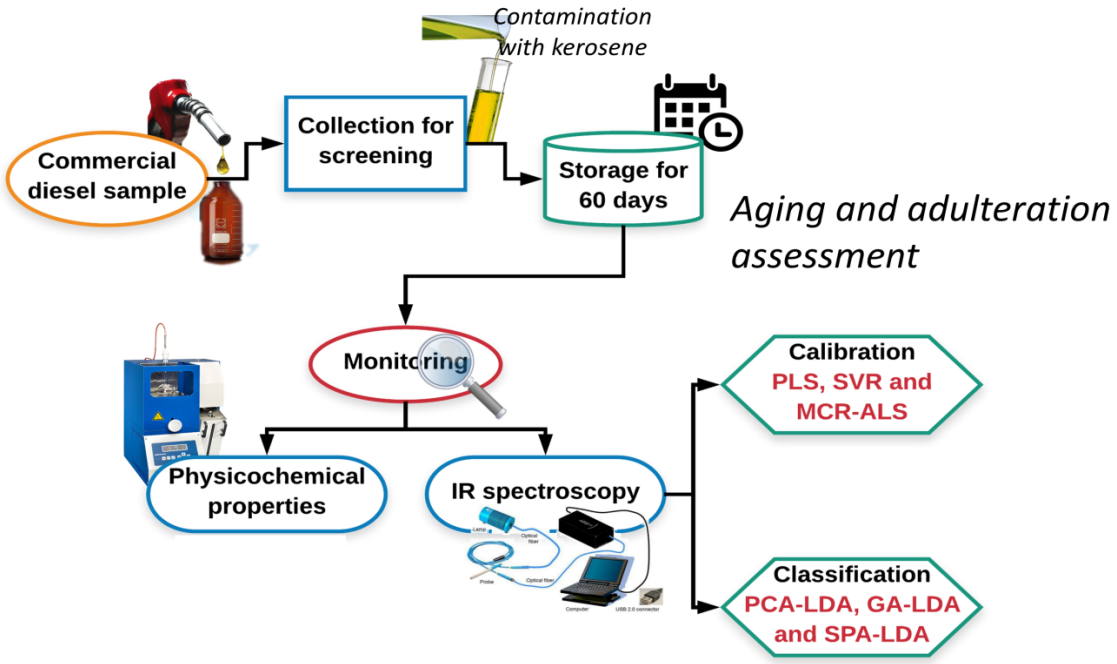


**Scheme 1.** Process flow diagram of the methodology used in this work.

## Chemometric Methods

### Exploratory Analysis (PCA) and Variable Selection Methods (SPA and GA)

Principal component analysis (PCA) is an unsupervised classification method that decomposes a data set into orthogonal variables called principal components (PCs). This reduces the size of the data while retaining the variance in the data set [25]. PCA is calculated based on the maximum variance contained in the dataset in a descending order of importance, where the first PC contains the larger explained variance, followed by the second, and so on. In addition, PCA solves collinearity problems to reduce the data size and improves efficacy to highlight and visualize the variations and heterogeneities among the samples. The PCA decomposition takes the form of [26]:

$$X = TP^T + E \quad (1)$$

where X is the spectral data set with n rows (samples) and m columns (wavelengths); T are the scores for all principal components a (a = 1, 2, 3, …, A), with size of n rows and A columns; P are the loadings for all principal components a, with size of m rows and A columns; and E is the residual matrix.

Successive projection algorithm (SPA) and genetic algorithm (GA) are techniques used as variables selection. SPA is a technique that considers each spectral variable as a vector. In this analysis, an initial vector (initial variable) is used. Then, new vectors with their respective projections are added in a subset orthogonal to that initial vector. In this way, the SPA selects those variables with more differentiated projections. With this, collinearity problems are eliminated [27]. GA, on the other hand, has a process that mimics the principle of Darwin's theory of evolution. In this technique, a population of variables is chosen randomly. This population is composed of subsets of variables. For each subset a fitness value is assigned through the fitness function present in the GA routine. Based on this fitness the subsets of variables can be eliminated or "survived" in a step called selection. Then, the genetic operators mutation and crossover are triggered, where initially selected variables may become unselected (mutation) and characteristics of one subset can pass to another (crossover). This procedure is called generation. There are as many generations as requested, and finally, the best fit subset will be the one with the selected variables [28]. The reduction of the multicollinearity problems obtained by SPA is done through the minimum of the cost function G. The fitness of GA is also calculated with this function, but in this case the fitness is calculated as the inverse of the cost function G, which is defined as:

$$G = \frac{1}{N_v}\sum_{N=1}^{N_v} g_n \quad (2)$$

with $g_n$ being described as:

$$g_n = \frac{r^2(x_n, m_{l(n)})}{min_{l(m)\neq l(n)} r^2(x_n, m_{l(m)})} \quad (3)$$

where the numerator is the square of the Mahalanobis distance between the object $x_n$ of the class $l_{(n)}$ and the mean of its true class $m_{l(n)}$; and the denominator is the square of the Mahalanobis distance between the object $x_n$ and the center of the nearest wrong class.

**Linear Discriminant Analysis (LDA)**

Linear discriminant analysis (LDA) is a supervised classification technique that improves the segregation level and reveals clusters that are maximized based on the separation between multiple classes rather than variations within each group [29]. Since PCA, SPA and GA are exploratory analysis methods, they are only able to show a distribution pattern between samples. On the other hand, LDA is a supervised classification method capable of making an exact differentiation between the different data groups. Thus, the scores are utilized as discriminant variables for LDA technique in order to create a linear decision boundary between them [30]. The LDA classification score takes the form of:

$$\mathrm{cf}(\mathrm{x}_i) = (\mathrm{x}_i - \mu_k)^{\mathrm{T}} \Sigma_{\mathrm{pooled}}^{-1} (\mathrm{x}_i - \mu_k) - 2 \ln \pi_k \quad (4)$$

where $\mathbf{x}_i$ is the measurement vector of sample *i*; $\mu_k$ is the mean of class *k*; $\Sigma_{\mathrm{pooled}}$ is the pooled covariance matrix; and $\pi_k$ is the prior probability of class *k*. These parameters are calculated as [30]:

$$\mu k = 1nki = 1nkxi \quad (5)$$

$$\Sigma_{\mathrm{pooled}} = \frac{1}{n} \sum_{k=1}^{K} n_k \Sigma_k \quad (6)$$

$$\Sigma_k = \frac{1}{n_k - 1} \sum_{i=1}^{n_k} (\mathrm{x}_i - \mu_k)(\mathrm{x}_i - \mu_k)^{\mathrm{T}} \quad (7)$$

$$\pi_k = \frac{n_k}{n} \quad (8)$$

where $\Sigma_k$ is the variance covariance matrix of class k; $n_k$ is the number of samples of class k; n is the total number of samples in the training set; and K is the number of classes.

**Calibration Models**

Partial least squares (PLS) regression is a multivariate calibration technique that finds factors (latent variables, LVs) in the spectra set that explain its maximum variance by using the simultaneous decomposition of the spectral and concentration matrices. The spectra set X and the concentration set y are decomposed as follows [31]:

$$\mathrm{X} = \mathrm{TP}^{\mathrm{T}} + \mathrm{E} \quad (9)$$

$$y = Uq^T + f \quad (10)$$

where T is the scores matrix of X; P is the loadings matrix of X; E is the residual matrix of X; U is the scores matrix of y; q is the loading vector of y; and f is the residual vector of y.

Support vector machines (SVM) is a supervised learning algorithm employed for training a computational system to recognize patterns and to perform further predictions. SVM for regression, called support vector regression (SVR) [32], is commonly employed in calibration problems for quantification purposes. SVR is based on estimating a response function for each sample spectrum as [33]:

$$f(x) = W\emptyset(x) + b \quad (11)$$

where the sample spectrum $x$ is non-linear mapped into a high-dimensional feature space $\mathbf{Z}$ by $W\emptyset(x)$, in which $\emptyset: x_i \rightarrow z_i$; and $b$ represents the bias parameters.

Multivariate curve resolution with alternating least squares (MCR-ALS) is a bilinear model that is the multi-wavelength extension from Lambert-Beer's law, and can be described by Equation 12 [34]:

$$D = CS^T + E \quad (12)$$

where D $(n \times m)$ is a data matrix containing the NIR or FTIR spectra of *n* samples for the *m* recorded wavelengths; C$(n \times A)$ and $S^T(A \times m)$ are the matrices with the concentration and spectra profiles of $A$ pure components in the samples, respectively. E has the same size as D and contains the unexplained variance from the bilinear model, related as the experimental error [35].

Some constraints must be applied to each iteration to reduce the number of possible solutions for C and $S^T$, and to give chemical meaning to the results. Non-negativity constraint was applied in this work. This constraint forces the concentration and/or spectral profile to be equal or larger than zero [36]. The correlation constraint allows the construction of a model with a univariate internal calibration from the scores calculated by MCR against the reference values concentration, being able to predict the concentration of calibration and unknown samples, and the concentration of these samples has to be in the analytical range of the calibration set [18].

**Figures of Merit (FOMs)**

In order to evaluate the predictive capacity and accuracy of multivariate calibration and classification models, a set of figures of merit was calculated (Table 2) [37].

**Table 2.** Equations for calculating FOMs.

| | |
|---|---|
| **Calibration** | |
| Root mean square error of prediction (RMSEP) | $RMSEP = \sqrt{\frac{\sum_{i=1}^{n}(y_i - \hat{y}_i)^2}{n}}$ |
| Standard error of prediction (SEP) | $SEP = \sqrt{\frac{\sum_{i=1}^{n}(y_i - \hat{y}_i)^2}{n}}$ |
| Bias | $bias = \frac{\sum_{i=1}^{n}(y_i - \hat{y}_i)}{n}$ |
| Relative percentage error in concentration prediction (RE%) | $RE(\%) = 100\sqrt{\frac{\sum_{i-1}^{n}(y_i - \hat{y}_i)^2}{\sum_{i=1}^{n} y_i{}^2}}$ |
| Root mean square error of cross-validation (RMSECV), | $RMSECV = \sqrt{\frac{\sum_{i=1}^{n}(y_p - y_e)^2}{n}}$ |
| **Classification** | |
| Sensitivity (SENS) | $SENS\,(\%) = \frac{TP}{TP + FN} \times 100$ |
| Specificity (SPEC) | $SPEC\,(\%) = \frac{TN}{TN + FP} x100$ |
| Correct classification (CC) | $CC(\%) = \frac{\{\sum y_1 + \sum y_2\}}{n} x100$ |

$n$: total number of samples in the set; $y_i$ and $\hat{y}_i$: actual and predicted concentrations in sample $I$; $y_p$ and $y_e$: predicted and expected concentration values; FN: false negative; FP: false positive; TP: true positive; TN: true negative; $y_1$ and $y_2$: number of samples incorrectly classified for each class.

## Results and Discussion

### Physicochemical Analysis

Fig. 1 depicts the results for the physicochemical evaluations. The distillation curves of samples with 0 and 15% kerosene performed on storage days 0 and 60 are indicated by Q0-0 and Q15-0 (Fig. 1a), Q0-60 and Q15-60 (Fig. 1b). Atmospheric distillation is one of the most important physicochemical properties to detect fuel adulteration in Brazil, and is based on the boiling temperature profile of the sample components [6]. Although the insertion of kerosene caused a slight decrease in boiling points of the intermediary hydrocarbon fraction of the blends, the temperatures obtained were still in accordance with ANP specifications for commercial diesel [5] and did not change over storage time.

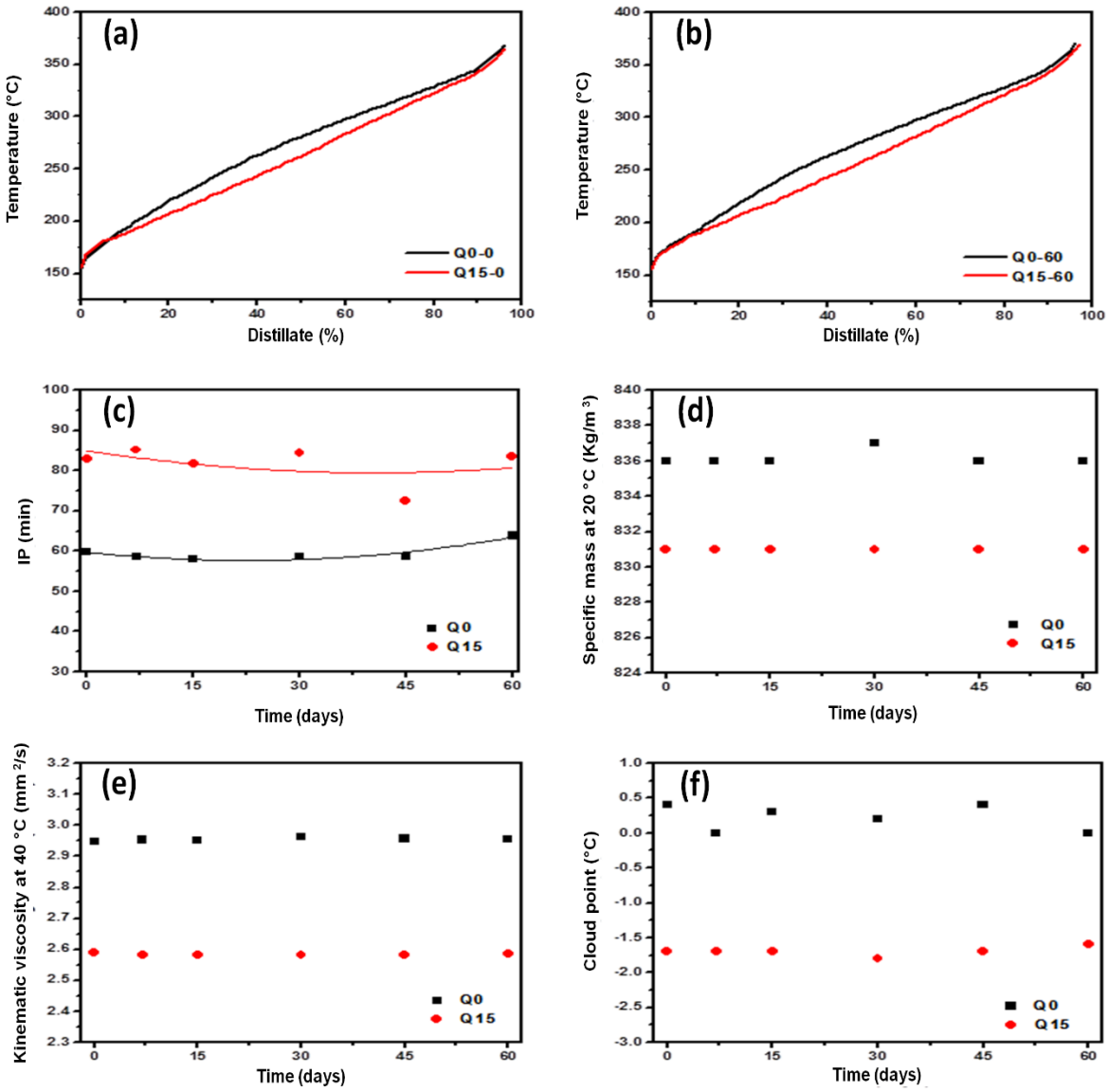


**Fig. 1.** Results for (a and b) atmospheric distillation, (c) PetroOxy, (d) specific mass at 20 °C, (e) kinematic viscosity at 40 °C and (f) cloud point tests for Q0 and Q15 samples during storage.

The induction period (IP) of Q0 and Q15 blends (Fig. 1c) remained within a range of little variability between days 0 and 60 [38]. The addition of 15% kerosene to S10B10 diesel increased the IP of the mixtures, probably due to the initial dilution of biodiesel in the S10B10 mixture, thus reducing the number of unsaturated molecules and ester groups available to react and form oxidized by-products [39]. The decrease in specific mass at 20 °C and kinematic viscosity at 40 °C values (Fig. 1d and 1e) with kerosene contamination is an effect of its relatively lighter composition in comparison to diesel, and promoting the dilution of denser and more viscous diesel-biodiesel

components [40]. The cloud point of the mixtures also decreased after adding kerosene (Fig. 1f) by simply diluting the paraffin waxes and biodiesel ester chains [41,42].

According to the results shown above in Fig. 1, none of the physicochemical properties evaluated in this work were able to detect changes in the characteristics of the diesel-biodiesel blends, either pure or kerosene, during storage. In addition, the contaminated diesel S10B10 samples remained within the quality parameters of ANP Resolution N° 30 and the adulteration would easily go unnoticed by a common physicochemical evaluation. Thus, chemometric tools were applied to IR data for elucidating these issues.

**Infrared Spectroscopy**

The spectra obtained by MIR and NIR analysis for samples with 0 to 40% (v/v) kerosene on the initial day of storage are shown in Fig. 2a and 2b, respectively.

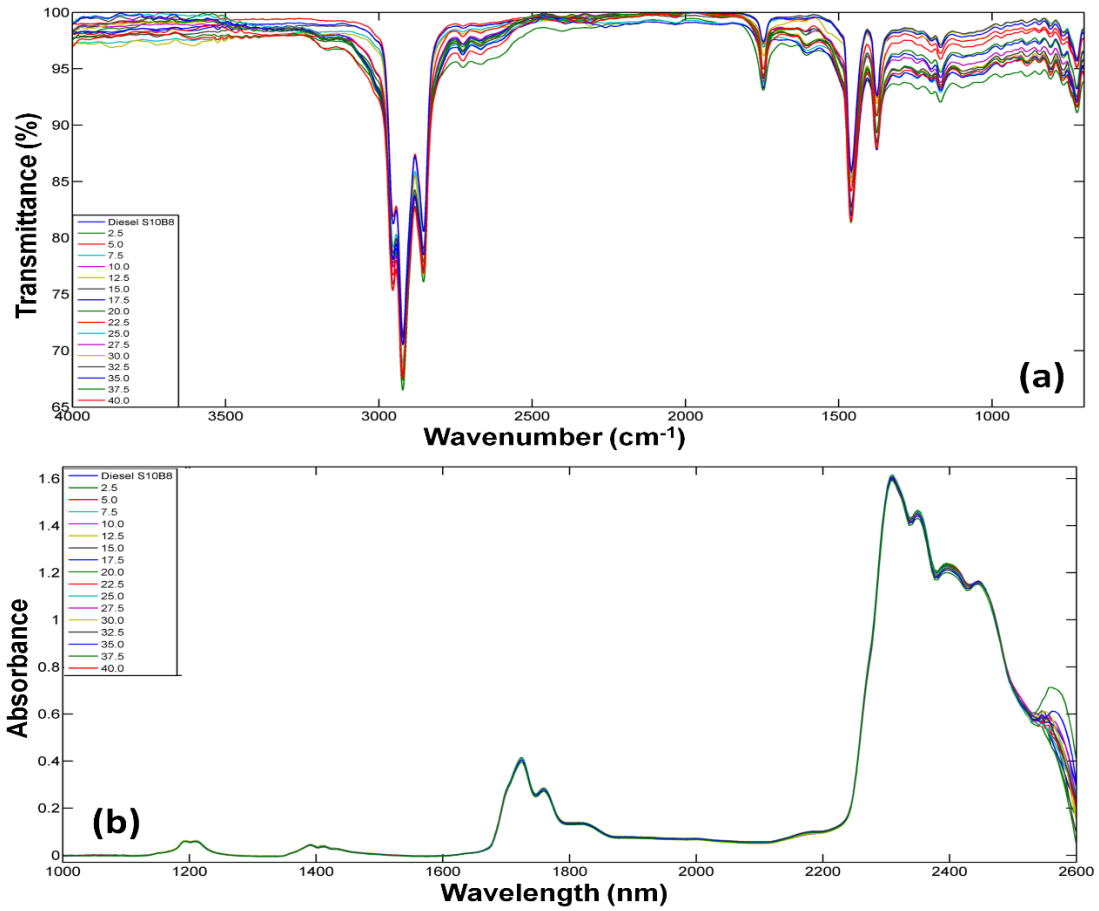


**Fig. 2.** (a) MIR and (b) NIR spectra for samples with 0 to 40% (v/v) kerosene on the first day of storage.

In the IR spectra (Fig. 2) there is the presence of some characteristic absorption features of biodiesel and the petroleum distillates. For MIR (Fig. 2a), the bands at 2952-2853 $cm^{-1}$ are related to anti-symmetric and symmetrical stretching modes of $CH_2$, $CH_3$ and CH biodiesel chains. The absorption feature at 1740 $cm^{-1}$ refers to C=O stretching mode of saturated aliphatic esters, and those occurring at 1196 and 1168 $cm^{-1}$ correspond to the C-O stretching mode of esters from the biodiesel. The bands at 1461 $cm^{-1}$, 1377 $cm^{-1}$ and 722 $cm^{-1}$ are referent to angular C-H bond deformations [43].

There are bands at 2130 nm and 2375 nm in the NIR spectra (Fig. 2b) referent to combination C-H/C=O stretching and C-H deformation bands, and a C-H stretch/C-C stretching combination band, respectively. In addition, there are band suppressions at 1690-1800 nm, 2150 nm, 2400 nm and 2450 nm, referent to the 1$^{st}$ overtone of $CH_2$ symmetric stretching, combination C–H stretching/C=O stretching, combination C-H stretching/C-C stretching forming CH, and combination C-H stretching/C-C stretching forming $CH_2$, respectively [44].

Although the increase of kerosene content in the samples promotes the biodiesel dilution (as can be seen in Fig. A1 of Online Resource 1), it does not linearly alter the intensity of the ester fingerprint region bands (2130 nm for NIR, 1740 $cm^{-1}$ for MIR), thus precluding univariate quantification.

**Multivariate Calibration for Kerosene Quantification**

As spectroscopic techniques do not resolve the components in a sample, chemical information about single components is embedded in multiple bands in the spectra and spectroscopic instruments alone provide very limited information toward unambiguous identification of unknown mixtures [6,45]. In this case, chemometric tools are commonly employed.

PLS regression was applied to the data using 4 LVs (99.94% explained variance) for MIR and 4 LVs (99.99% explained variance) for NIR data. SVR calibration models were obtained using 9 support vectors (SVs) for NIR and 11 SVs for MIR. Thus, the SVR model was obtained using *C* (100), *m* (0.01) and Gamma (10) parameters, for both techniques, in order to find the best RMSEC value. The use of adequate parameters allows the adjustment of the *e*-insensitive loss function and the *e*-tube, which prevents the model from overfitting [33]. The measured *versus* predicted concentration of kerosene (%) plots of PLS and SVR calibration models are found in the Online Resource 1. Results for FOMs are depicted in Table 3.

**Table 3.** Figures of merit (FOMs) for PLS and SVR calibration models.

| Model | FOM | MIR | | | NIR | | |
|---|---|---|---|---|---|---|---|
| PLS | | Calibration | Cross-validation | Prediction | Calibration | Cross-validation | Prediction |
| | RMSE (%) | 2.35 | 2.35 | 3.21 | 2.59 | 2.59 | 3.74 |
| | Bias (%) | -0.19 | -0.01 | 0.12 | 0.00 | $5.61 \times 10^{-5}$ | -3.61 |
| | RE (%) | 10.21 | - | 12.14 | 11.09 | - | 14.48 |
| | $R^2$ | 0.959 | 0.964 | 0.926 | 0.951 | 0.951 | 0.991 |
| | *t*-test* | - | - | 2.774 | - | - | 2.306 |
| | F-test* | - | - | 1.120 | - | - | 1.051 |
| SVR | RMSE (%) | 0.43 | 5.99 | 3.85 | 0.63 | 5.08 | 5.56 |
| | Bias (%) | 0.104 | 0.03 | -2.99 | -0.22 | -1.26 | 3.16 |
| | RE (%) | 2.00 | - | 11.18 | 3.26 | - | 19.99 |
| | $R^2$ | 0.999 | 0.714 | 0.988 | 0.998 | 0.784 | 0.999 |
| | *t*-test* | - | - | 2.446 | - | - | 2.776 |
| | F-test * | - | - | 0.999 | - | - | 1.028 |

*Tabulated value of t = 2.776; Critical F = 3.717 at 95% confidence level.

The PLS model for MIR data shows satisfactory performance for quantifying the kerosene content in the adulterated samples, with a root mean square error of cross-validation (RMSECV) and prediction (RMSEP) equal to 2.35% and 3.21%, respectively. Additionally, the model shows to be linear in the concentration range ($R^2$ = 0.947). Similar results are observed for NIR data, where the RMSECV and RMSEP were respectively equal to 2.59% and 3.74%. The growth in the residues is associated with the higher complexity of NIR data in comparison with MIR. The NIR spectra are composed of superposed overtone and combinations bands; whereas the MIR spectra are associated to fundamental vibration modes of the samples' constituents, therefore being more sensible [6]. The SVR-NIR model presents a constant variance and low residues for both calibration and prediction samples, with a root mean square error of cross-validation (RMSECV) and prediction (RMSEP) equal to 5.07% and 5.56%, respectively, and a determination coefficient of 0.999. The same behavior occurs in SVR-MIR, where the RMSECV and RMSEP were equal to 3.85% and 5.99%, respectively, in addition to a determination coefficient of 0.988, which indicates good fit throughout the analytical ranges for both methods.

The values of calibration, cross-validation and prediction errors obtained for this methodology are close to those observed in the literature for quantifying kerosene in diesel by another spectroscopic technique [46]. Results of paired t-tests and F-tests (Table 3) confirm that predicted concentrations were statistically equal to the reference concentrations and all the calibration models used in this work are valid for a confidence level of 95%. The low RMSE values and the high correlation coefficients demonstrate that these PLS models may be applied to quantify

kerosene volumetric concentration in diesel for controlling adulteration issues. Fig. 3 depicts the elliptical joint confidence region (EJCR) at 95% confidence level for the slope and intercept of the regression line in predicted versus reference values. The ellipse contains the ideal point (1,0) for slope and intercept, respectively, showing that the reference and predicted values are not significantly different at 95% confidence level for PLS-MIR, PLS-NIR, SVR-NIR and SVR-MIR; thus, no systematic errors were detected in calibration.

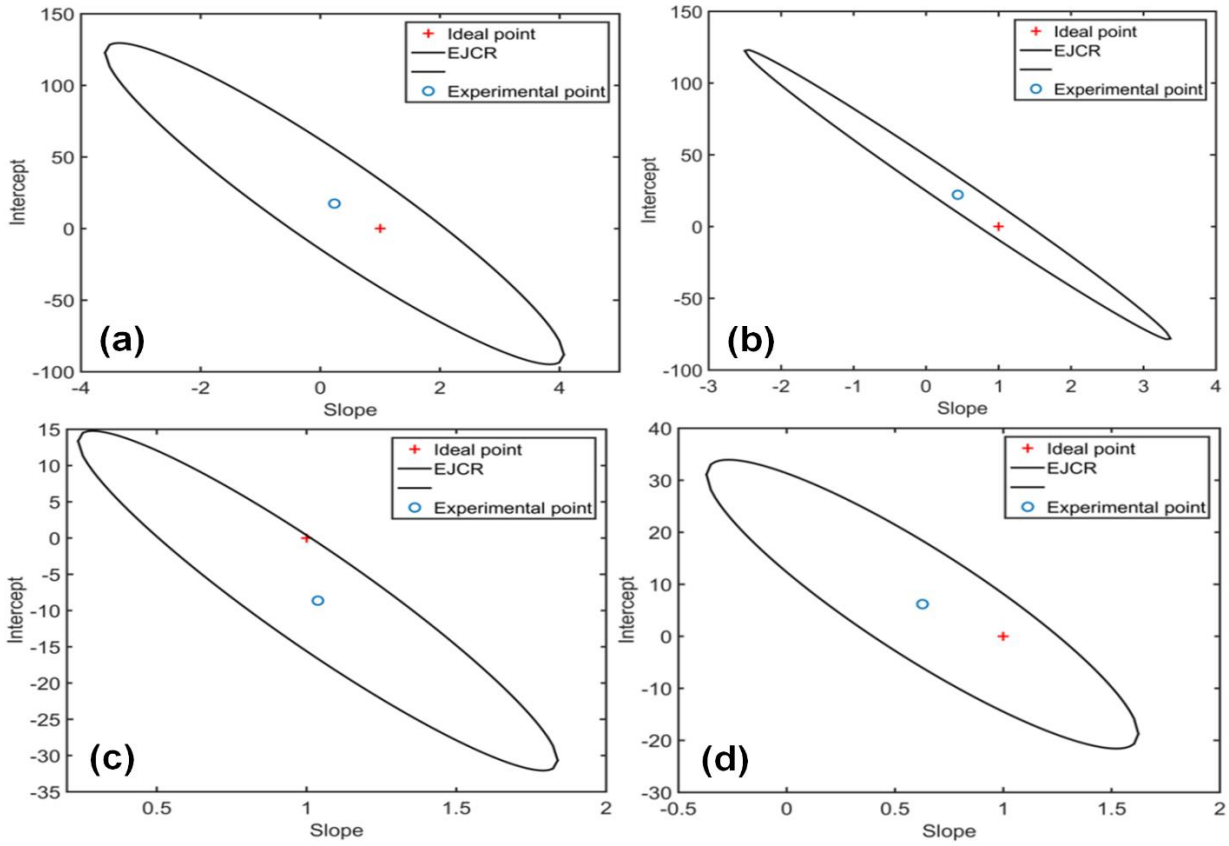


**Fig. 3.** EJCR for the calibrations models to quantifying kerosene with (a) PLS-MIR, (b) SVR-MIR, (c) PLS-NIR and (d) SVR-NIR.

MCR-ALS was also applied to these data; however, it was not possible to quantify the concentration of kerosene with IR spectroscopy due to the non-correlation between samples. A low correlation coefficient and high errors were obtained for MIR, such as RMSEC and $R^2$ of 20.79% and 0.470, respectively. Meanwhile, the recovered spectral profile (Sopt) of the adulterant could be calculated and is shown in Fig. 4a.

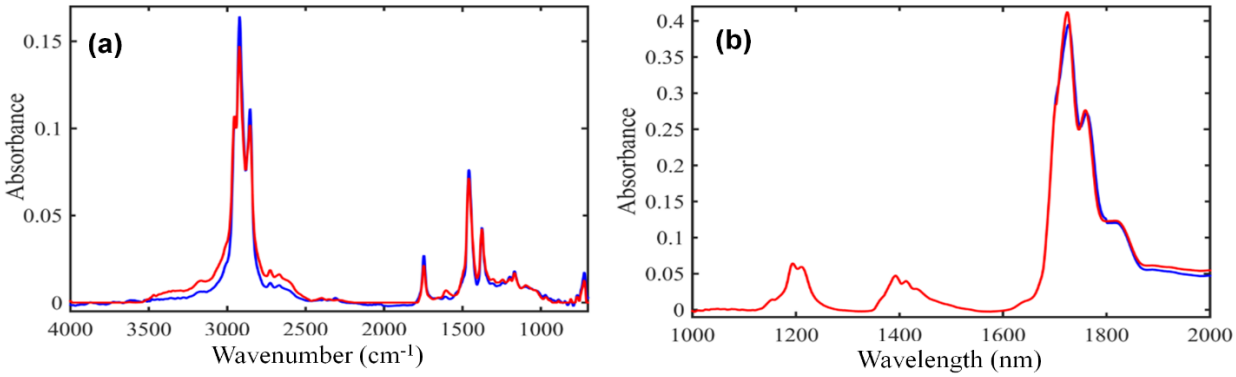


**Fig. 4.** Comparison between the original IR spectra (blue) and the Sopt obtained by MCR-ALS (red) for kerosene solvent using (a) MIR and (b) NIR data.

The model was able to recover 3 Sopts, where Sopt1, Sopt2 and Sopt3 are the recovered profiles of diesel S10, kerosene and biodiesel, respectively, identifying the adulterant spectra despite the high chemical similarity between diesel and kerosene. This can be concluded because of the similarity between the spectral profiles and Sopts, presenting only a small difference in some band intensities due to the resemblance among the fuel and the adulterant. MCR-NIR presented lower RMSEC and higher $R^2$ values than MCR-MIR (15.94% and 0.620, respectively). These results indicate better precision in the quantification process; meanwhile, this model is not reliable for quantifying kerosene content and may only be used for the Sopt recuperation (Fig. 4b). It was possible to recover two spectral profiles (Sopt1 and Sopt2), corresponding to the diesel/biodiesel blend and kerosene, respectively.

Correlation analysis ($R^2$) between kerosene spectra and the recovered profile was also performed and showed the resemblance among them. The $R^2$ was of 0.977 and 0.990 for MCR-MIR and MCR-NIR. This method can be interesting to solve the big issue of identifying kerosene adulteration in commercial diesel, along with PLS and SVR calibration to efficiently quantify its content.

**Multivariate Classification for Fuel Aging**

By applying PCA to the preprocessed data, three PCs (87.53% of explained variance) were selected for MIR and three PCs (96.67% of explained variance) for NIR. Fig. 5 depicts the scores graph for the PCA models without LDA. The scores graph that best separated the sample classes under and over 30 days of storage in PCA was built using PC2 x PC3 for MIR and PC1 x PC2 for NIR (Fig. 5a and 5b). PCA was able to separate the samples with aging time

over and under 30 days of storage using MIR spectral data (Fig. 5a), detecting some compositional differences caused by the aging process to distinguish both classes. For NIR (Fig. 5b), group distribution was not satisfactory just with the exploratory analysis. Since PCA is used to get a view of the data in space and the important loadings for each PC, LDA is needed for enabling an accurate classification of the samples.

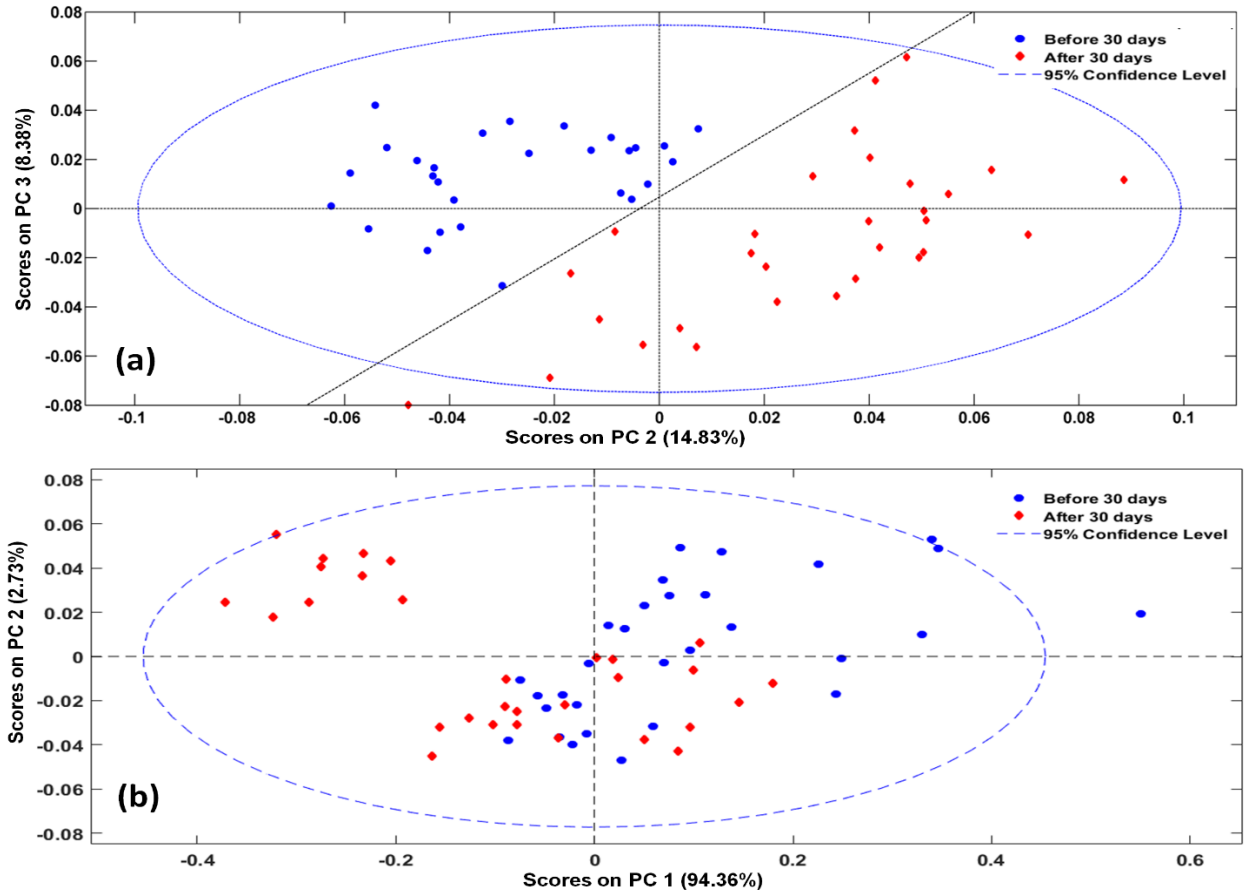


**Fig. 5.** Scores plot for (a) MIR and (b) NIR spectra analyzed by PCA.

The loadings profile of PCA-MIR model (Fig. 6) depicts the absorption features of the IR spectra that most influenced the segregation between the sample classes. The coefficients that most influenced PC1 were wavenumbers at 1740 $cm^{-1}$, 1196 $cm^{-1}$and 1168 $cm^{-1}$, referent to biodiesel absorption bands (see Fig. 2a). This occurs since biodiesel is composed of esters, which have different spectroscopic characteristics than the hydrocarbons present in diesel and kerosene. Thus, the pattern recognition model was able to detect the influence of kerosene by the changes in biodiesel content into the blends. It can be proposed that PC1 was able to identify the influence of the increasing content of kerosene adulterant in the storage stability and in the degradation process of

the samples, as predicted by PetroOxy results. PC2 and PC3 were more influenced by wavenumbers that correspond to compounds that may have been produced in the degradation of the blends, such as aldehydes, phenols and amides (see Table 4), which justifies the good separation of classes with different storage times in the PCA scores (Fig. 5a).

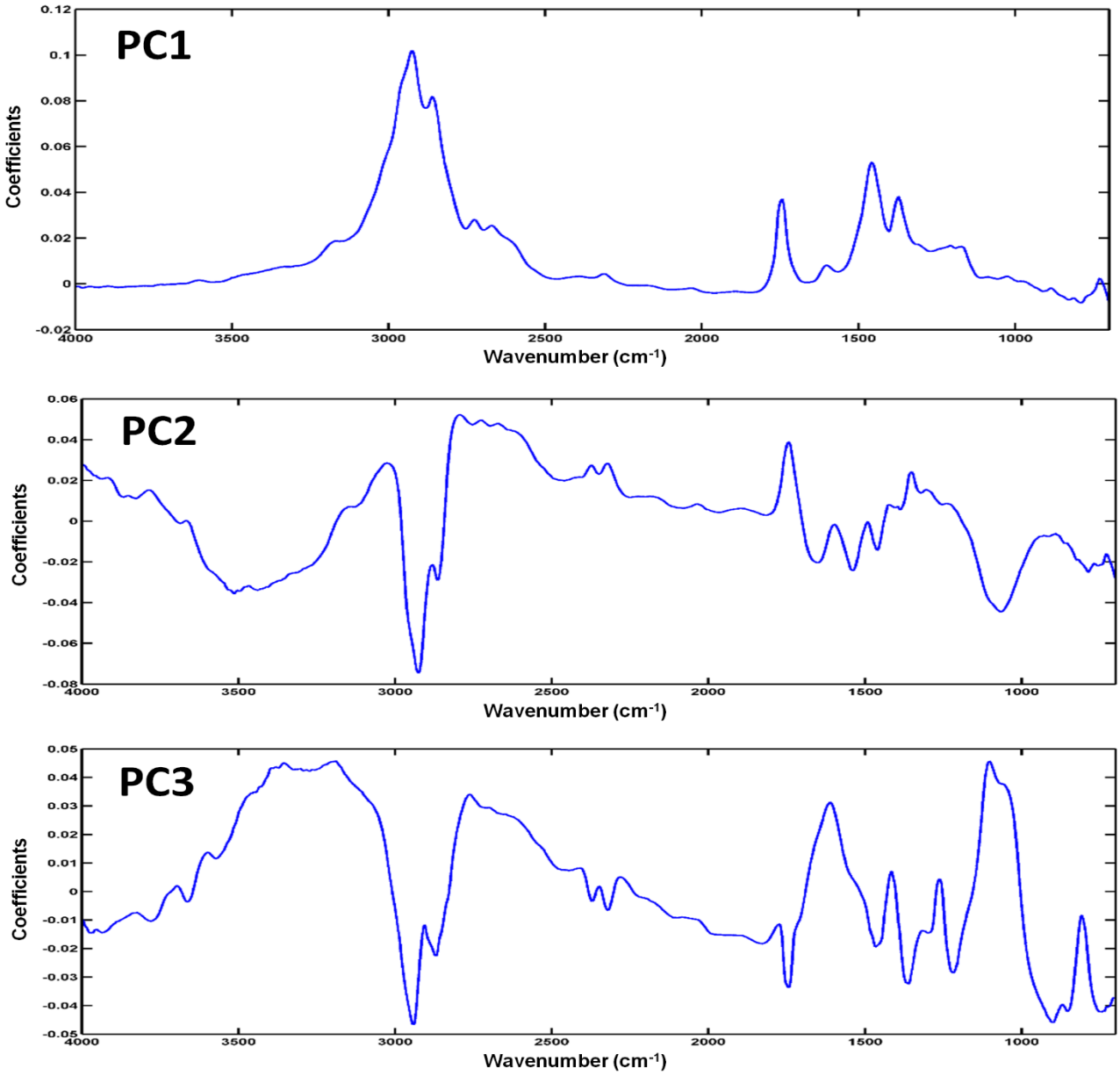


**Fig. 6.** PCA loadings profile for MIR.

**Table 4.** Absorption features that most influenced PC2 and PC3 in MIR loadings.

| Positive coefficients of PC2 | | Negative coefficients of PC2 | |
|---|---|---|---|
| Wavenumber ($cm^{-1}$) | Vibration | Wavenumber ($cm^{-1}$) | Vibration |
| 3070-3010 | Aromatic ν(C-H) | 3500 | O-H |
| 2800-2700 | Aldehyde ν(C-H) | 2921 | ν(C-H) of $CH_2$ |
| 1800-1700 | ν(C=O) | 2853 | ν(C-H) of $CH_2$ |
| | | 1600-1450 | Aromatic ν(C=C) |
| | | 1060-1020 | ν(C=S) or ν(S=O) |
| **Positive coefficients of PC3** | | **Negative coefficients of PC3** | |
| Wavenumber ($cm^{-1}$) | Vibration | Wavenumber ($cm^{-1}$) | Vibration |
| 3300 | Carboxylic acid ν(O-H) or amide ν(N-H) | 2921 | ν(C-H) of $CH_2$ |
| 2800-2700 | Aldehyde ν(C-H) | 2853 | ν(C-H) of $CH_2$ |
| 1560-1530 | Amide δ(N-H) and ν(C-N) | 1800-1700 | ν(C=O) |
| 1060-1020 | ν(S=O) | 1250 | ν(C-O) |
| | | 722 | $\rho_{as}$(C-H) of $CH_2$ |

ν: axial deformation; δ: angular deformation; $\rho_{as}$: asymmetric deformation at the plane.

In PCA-LDA, 10 PCs were selected for MIR and NIR (96.53% and 97.87% of explained variance, respectively) to classify the data according to its storage time (over and under 30 days of storage). SPA and GA algorithms provide a set of selected variables that promotes the higher inter-class segregation to be used in LDA. The selected variables for both SPA and GA are shown in Table 5. All the discriminant function (DF) plots for the models are presented on Online Resource 2.

**Table 5.** SPA and GA selected variables for MIR and NIR data.

| Spectroscopic technique | Model | Selected variables |
|---|---|---|
| MIR ($cm^{-1}$) | SPA (34)[a] | 698 745 779 810 854 907 999 1204 1321 1360 1398 1422 1445 1485 1533 1578 1663 1721 1748 1794 2280 2336 2791 2886 2938 2959 3005 3518 3545 3651 3686 3794 3906 3998 |
| | GA (26)[a] | 1022 1047 1059 1092 1142 1167 1254 1346 1416 1528 1744 1746 2045 2095 2253 2452 2675 2806 2860 2997 3009 3096 3406 3688 3711 3993 |
| NIR (nm) | SPA (31)[a] | 922 925 928 934 941 946 953 957 964 966 973 983 987 997 1008 1017 1026 1035 1048 1095 1139 1238 1387 1411 1673 1689 1705 1765 1852 1926 2133 |
| | GA (27)[a] | 954 977 1033 1065 1096 1152 1154 1160 1168 1244 1265 1309 1340 1356 1378 1397 1437 1478 1528 1660 1696 1748 1799 1814 1833 1926 2108 |

[a] number of selected variables.

As also seen in PCA loadings (Table 4) for the model with good aging classification before applying LDA (PCA-MIR), some of the SPA and GA selected variables for MIR and NIR are related to biodiesel content (~1748 $cm^{-1}$ for MIR and ~2133 nm for NIR, for example)and probable products of sample degradation, such as aldehydes (1700-1800 $cm^{-1}$ for MIR), amides (~1530 $cm^{-1}$ for MIR and ~1430 nm for NIR) and carboxylic acids (~1700 $cm^{-1}$ for MIR and ~1920 nm for NIR) [43,47]. After this selection, LDA was applied in order to classify the samples into their correct classes. Sensitivity (Sens), specificity (Spec) and correct classification (CC) were calculated in order to infer the prediction performance for these models. Table 6 summarizes the results for figures of merit for the classification models. PCA-LDA and SPA-LDA reached 100% accuracy with both IR methods; although GA-LDA presented some lower results of sensitivity and correct classification for the sample class before 30 days of storage, its efficiency was still satisfactory (>85.7%).

**Table 6.** Figures of merit (FOMs) inferred for the classification work with PCA-LDA, SPA-LDA and GA-LDA models.

| Spectroscopic technique | FOM | PCA-LDA | SPA-LDA | GA-LDA |
|---|---|---|---|---|
| MIR | Before 30 days | | | |
| | Sens (%) | 100.0 | 100.0 | 85.7 |
| | Spec (%) | 100.0 | 100.0 | 100.0 |
| | CC (%) | 100.0 | 100.0 | 91.6 |
| | After 30 days | | | |
| | Sens (%) | 100.0 | 100.0 | 100.0 |
| | Spec (%) | 100.0 | 100.0 | 100.0 |
| | CC (%) | 100.0 | 100.0 | 100.0 |
| NIR | Before 30 days | | | |
| | Sens (%) | 100.0 | 100.0 | 85.7 |
| | Spec (%) | 100.0 | 100.0 | 100.0 |
| | CC (%) | 100.0 | 100.0 | 91.6 |
| | After 30 days | | | |
| | Sens (%) | 100.0 | 100.0 | 100.0 |
| | Spec (%) | 100.0 | 100.0 | 100.0 |
| | CC (%) | 100.0 | 100.0 | 100.0 |

These results show that PCA-LDA, SPA-LDA and GA-LDA models for both IR spectroscopies are capable of differentiating the monthly storage time of these fuels with good accuracy, unlike what can be observed in the physicochemical analysis results during storage, which were not able to detect changes in diesel-biodiesel samples with or without kerosene during the monitoring. Furthermore, NIR data can be recorded by portable instruments, enabling faster “in loco” inspection procedures with an effective and simple methodology with the combined classification models. PCA loadings detected the presence of adulteration by observing variations on biodiesel concentration, in addition to detect chemical species from decomposition reactions of the diesel-biodiesel-kerosene mixtures as the main features responsible for aging class separation, as well as SPA and GA selected variables.

## Conclusions

The NIR and MIR spectra coupled to PLS and SVR models for quantifying kerosene content presented low RMSE values and high correlation between real and predicted concentrations, in spite of the similar chemical composition

of diesel and kerosene. MCR-ALS with correlation constraint was able to identify and recover the spectral profile of commercial diesel and kerosene adulterant from the IR spectra of contaminated blends.

PCA-LDA, SPA-LDA and GA-LDA enabled correctly classifying diesel-biodiesel with kerosene in different degradation levels, separating these samples into two well-defined groups under and over thirty days of storage. The method was highly accurate and reliable for evaluating fuel storage stability. PCA loadings, as well as GA and SPA selected variables, detected that spectroscopic features related to degradation products such as amides, carboxylic acids and aldehydes were responsible for the classification by aging stage.

The multivariate classification methodology developed in this paper is an efficient tool for classifying commercial diesel with kerosene adulterant by aging time and chemically observe the degradation phenomenon. Combining MCR-ALS with PLS or SVR models is powerful to solve the great issue in quantifying and identifying this adulteration, being interesting to improve the investigative process of adulteration in diesel fuel screening. The results of the study that we performed demonstrated good results in the quantification using these techniques. However, more in-depth studies with more sampling need to be performed in order to have a better validation of the technique and to be more certain. However, our results are encouraging. The evaluation method is simple, fast, does not require pretreatment of the samples, may be carried out "in loco" with portable NIR instruments and is low cost.

## Acknowledgements

The authors acknowledge the support provided by the Post-Graduate Chemistry Program PPGQ/UFRN, the Energetic Technologies Laboratory (LTEN), the Biological Chemistry and Chemometrics Group, the CAPES and CNPQ – Brazil for the financial support.

## Conflict of Interest

The authors declare that they have no conflict of interest.

## References

[1] Obeidat SM, Al-Ktash MM, Al-Momani IF. Study of fuel assessment and adulteration using EEMF and multiway PCA. Energy Fuels. 2014; https://doi.org/10.1021/ef500718e [CrossRef] [Google Scholar]

[2] Krakowska B, Stanimirova I, Orzel J, Daszykowski M, Grabowski I, Zaleszczyk G, Sznajder M. Detection of discoloration in diesel fuel based on gas chromatographic fingerprints. Anal Bioanal Chem. 2015; https://doi.org/10.1007/s00216-014-8332-4 [CrossRef] [Google Scholar]

[3] Agência Nacional do Petróleo, Gás Natural e Biocombustíveis – ANP. Resolução No. 3 de 08.02.2007. In: DOU 09.02.2007. http://legislacao.anp.gov.br/?path=legislacao-anp/resol-anp/2007/fevereiro&item=ranp-3--2007&export=pdf. Accessed in 20 Oct 2018.

[4] Menezes EW, Silva R, Cataluña R, Ortega RJC. Effect of ethers and ether/ethanol additives on the physicochemical properties of diesel fuel and on engine tests. Fuel. 2006; https://doi.org/10.1016/j.fuel.2005.08.027 [CrossRef] [Google Scholar]

[5] Agência Nacional do Petróleo, Gás Natural e Biocombustíveis – ANP. Resolução No. 30 de 23.06.2016. In: DOU 24.06.2016. http://www.lex.com.br/legis_27160107_RESOLUCAO_N_30_DE_23_DE_JUNHO_DE_2016.aspx. Accessed in 20 Oct 2018.

[6] Câmara ABF, de Carvalho LS, Morais CLM, Lima LAS, Araújo HOM, Oliveira FM, Lima KMG. MCR-ALS and PLS coupled to NIR/MIR spectroscopies for quantification and identification of adulterant in biodiesel-diesel blends. Fuel. 2017; https://doi.org/10.1016/j.fuel.2017.08.072 [CrossRef] [Google Scholar]

[7] Cunha IBS, Fernandes AMAP, Tega DU, Simas RC, Nascimento HL, Sá GF, Daroda RJ, Eberlin MN, Alberici RM. Quantitation and quality control of biodiesel/petrodiesel (Bn) blends by easy ambient sonic-spray ionization mass spectrometry. Energy Fuels. 2012; https://doi.org/10.1021/ef3010866 [CrossRef] [Google Scholar]

[8] Gotor R, Tiebe C, Schilischka J, Bell J, Rurack K. Detection of adulterated diesel using fluorescent test strips and smartphone readout. Energy Fuels. 2017; https://doi.org/10.1021/acs.energyfuels.7b01538 [CrossRef] [Google Scholar]

[9] Jose TK, Anand K. Effects of biodiesel composition on its long term storage stability. Fuel. 2016; https://doi.org/10.1016/j.fuel.2016.03.007 [CrossRef] [Google Scholar]

[10] Brereton RG, Jansen J, Lopes J, Marini F, Pomerantsev A, Rodionova O, Roger JM, Walczak B, Tauler R. Chemometrics in analytical chemistry – part II: modeling, validation, and applications. Anal Bioanal Chem. 2018; https://doi.org/10.1007/s00216-018-1283-4 [CrossRef] [Google Scholar]

[11] Zhang J, Wei X, Huang J, Lin H, Deng K, Li Z, Shao Y, Zou D, Chen Y, Huang P, Wang Z. Attenuated total reflectance Fourier transform infrared (ATR-FTIR) spectral prediction of postmortem interval from vitreous humor samples. Anal Bioanal Chem. 2018; https://doi.org/10.1007/s00216-018-1367-1 [CrossRef] [Google Scholar]

[12] Aboualizadeh E, Ranji M, Sorenson CM, Sepehr R, Sheibani N, Hirschmugl CJ. Retinal oxidative stress at the onset of diabetes determined by synchrontron FTIR widefield imaging: towards diabetes pathogenesis. Analyst. 2017; https://doi.org/10.1039/c6an02603f [CrossRef] [Google Scholar]

[13] Theophilou G, Morais CLM, Halliwell DE, Lima KMG, Drury J, Martin-Hirsch PL, Stringfellow HF, Hapangama DK, Martin FL. Synchrotron- and focal plane array-based Fourier-transform infrared spectroscopy differentiates the basalis and functionalis epithelial endometrial regions and identifies putative stem cell regions of human endometrial glands. Anal Bioanal Chem. 2018; https://doi.org/10.1007/s00216-018-1111-x [CrossRef] [Google Scholar]

[14] Marques AS, Moraes EP, Júnior MAA, Moura AD, Neto VFA, Neto RM, Lima KMG. Rapid discrimination of *klebsiella pneumoniae* carbapenemase 2 – producing and non-producing *klebsiella pneumoniae* strains using near-infrared spectroscopy (NIRS) and multivariate analysis. Talanta. 2015; https://doi.org/10.1016/j.talanta.2014.11.006 [CrossRef] [Google Scholar]

[15] Hu J, Ma X, Liu L, Wu Y, Ouyang J. Rapid evaluation of the quality of chestnuts using near-infrared reflectance spectroscopy. Food Chem. 2017; https://doi.org/10.1016/j.foodchem.2017.03.127 [CrossRef] [Google Scholar]

[16] Corgozinho CNC, Pasa VMD, Barbeira PJS. Determination of residual oil in diesel oil by spectrofluorimetric and chemometric analysis. Talanta. 2008; https://doi.org/10.1016/j.talanta.2008.03.003 [CrossRef] [Google Scholar]

[17] Thissen U, Pepers M, Ustun B, Melssen WJ, Buydens LMC. Comparing support vector machines to PLS for spectral regression applications. Chem Intell Lab Syst. 2004; https://doi.org/10.1016/j.chemolab.2004.01.002 [CrossRef] [Google Scholar]

[18] Dantas WFC, Alves JCL, Poppi RJ. MCR-ALS with correlation constraint and Raman spectroscopy for identification and quantification of biofuels and adulterants in petroleum diesel. Chemom Intell Lab Syst. 2017; https://doi.org/10.1016/j.chemolab.2017.04.002 [CrossRef] [Google Scholar]

[19] de Juan A, Tauler R. Multivariate curve resolution (MCR) from 2000: progress in concepts and applications. Crit Rev Anal Chem. 2006; https://doi.org/10.1080/10408340600970005 [CrossRef] [Google Scholar]

[20] ASTM D 7545-14. Standard test method for oxidation stability of middle distillate fuels – rapid small scale oxidation test (RSSOT). In: West Conshohocken (PA): ASTM International. 2014; https://www.astm.org/Standards/D7545.htm. Accessed 23 Oct 2018.

[21] ASTM D 86-12. Standard test method for distillation of petroleum products at atmospheric pressure. In: West Conshohocken (PA): ASTM International. 2013; https://www.astm.org/DATABASE.CART/HISTORICAL/D86-12.htm. Accessed 23 Oct 2018.

[22] ASTM D 7042-14. Standard test method for dynamic viscosity and density of liquids by Stabinger viscometer (and the calculation of kinematic viscosity). In: West Conshohocken (PA): ASTM International. 2014; https://www.astm.org/DATABASE.CART/HISTORICAL/D7042-14.htm. Accessed 23 Oct 2018.

[23] ASTM D 2500-11. Standard test method for cloud point of petroleum products. In: West Conshohocken (PA): ASTM International. 2011; https://www.astm.org/DATABASE.CART/HISTORICAL/D2500-11.htm. Accessed 23 Oct 2018.

[24] Kennard RW, Stone LA. Computer aided design of experiments. Technometrics. 1969; https://doi.org/10.2307/1266770 [CrossRef] [Google Scholar]

[25] Bro R, Smilde AK. Principal component analysis. Anal. Methods. 2014; https://doi.org/10.1039/C3AY41907J [CrossRef] [Google Scholar]

[26] Eftekhari A, Forouzanfar M, Moghaddam HA, Alirezaie J. Block-wise 2D kernel PCA/LDA for face recognition. Inform Process Lett. 2010; https://doi.org/10.1016/j.ipl.2010.06.006 [CrossRef] [Google Scholar]

[27] Pontes MJC, Galvão RKH, Araújo MCU, Moreira PNT, Neto ODP, José GE, Saldanha TCB. The successive projections algorithm for spectral variable selection in classification problems. Chemom Intell Lab Syst. 2005; https://doi.org/10.1016/j.chemolab.2004.12.001 [CrossRef] [Google Scholar]

[28] Broadhursta D, Goodacrea R, Jones A, Rowland JJ, Kell DB. Genetic algorithms as a method for variable selection in multiple linear regression and partial least squares regression, with applications to pyrolysis mass spectrometry. Anal Chim Acta. 1997; https://doi.org/10.1016/S0003-2670(97)00065-2 [CrossRef] [Google Scholar]

[29] Dixon SJ, Brereton RG. Comparison of performance of five common classifiers represented as boundary methods: Euclidean distance to centroids, linear discriminant analysis, quadratic discriminant analysis, learning

vector quantization and support vector machines, as dependent on data structure. Chemometr Intell Lab Syst. 2009; https://doi.org/10.1016/j.chemolab.2008.07.010 [CrossRef] [Google Scholar]

[30] Wu W, Mallet Y, Walczak B, Penninckx W, Massart DL, Heuerding S. Erni F. Comparison of regularized discriminant analysis, linear discriminant analysis and quadratic discriminant analysis. Applied to NIR data. Anal Chim Acta 1996; https://doi.org/10.1016/0003-2670(96)00142-0 [CrossRef] [Google Scholar]

[31] Geladi P, Kowalski BR. Partial least-squares regression: a tutorial. Anal. Chim. Acta**.** 1986; https://doi.org/10.1016/0003-2670(86)80028-9 [CrossRef] [Google Scholar]

[32] Smola AJ, Schölkopf B. A tutorial on support vector regression. Stat. Comput. 2004; https://doi.org/10.1023/B:STCO.0000035301.49549.88 [CrossRef] [Google Scholar]

[33] Alves JCL, Henriques CB, Poppi RJ. Determination of diesel quality parameters using support vector regression and near infrared spectroscopy for an in-line blending optimizer system. Fuel. 2012; https://doi.org/10.1016/j.fuel.2012.03.016 [CrossRef] [Google Scholar]

[34] Tauler R, Kowaslki B, Fleming S. Multivariate curve resolution applied to spectral data from multiple runs of an industrial process. Anal Chem. 1993; https://doi.org/10.1021/ac00063a019 [CrossRef] [Google Scholar]

[35] Jaumot J, Igne B, Anderso CA, Drennen JK, de Juan A. Blending process modeling and control by multivariate curve resolution. Talanta. 2013; https://doi.org/10.1016/j.talanta.2013.09.037 [CrossRef] [Google Scholar]

[36] Bro R, de Jong S. A fast non-negativity-constrained least squares algorithm. J Chemom. 1997; https://doi.org/10.1002/(SICI)1099-128X(199709/10)11:5<393::AID-CEM483>3.0.CO;2-L [CrossRef] [Google Scholar]

[37] Olivieri AC, Faber NM, Ferré J, Boqué R, Kalivas JH. Mark, H. Uncertainty estimation and figures of merit for multivariate calibration. Pure Appl Chem. 2006; https://doi.org/10.1351/pac200678030633 [CrossRef] [Google Scholar]

[38] Botella L, Bimbela F, Martin L, Arauzo J, Sanchez JL. oxidation stability of biodiesel fuels and blends using the Rancimat and PetroOxy methods. Effect of 4-allyl-2,6-dimetoxiphenol and cathecol as biodiesel additives on oxidation stability. Front Chem. 2014; https://doi.org/10.3389/fchem.2014.00043 [CrossRef] [Google Scholar]

[39] Karavalakis G, Stournas S, Karonis D. Evaluation of the oxidation stability of diesel/biodiesel blends. Fuel. 2010; https://doi.org/10.1016/j.fuel.2010.03.041 [CrossRef] [Google Scholar]

[40] Roy MM, Wang W, Alawi M. Performance and emissions of a diesel engine fueled by biodiesel-diesel, biodiesel-diesel-additive and kerosene-biodiesel blends. Energ Convers Manage. 2014; https://doi.org/10.1016/j.enconman.2014.04.033 [CrossRef] [Google Scholar]

[41] Yadav SR, Murthy KV, Mishra D, Baral B. Estimation of petrol and diesel adulteration with kerosene and assessment of usefulness of selected automobile fuel quality test parameters. IJEST. 2005; https://doi.org/10.1007/BF03325839 [CrossRef] [Google Scholar]

[42] Ziegler K, Manka J. The effect of mixing diesel fuels additized with kerosene and cloud point depressants. SAE Technical Paper 2000-01-2884. 2000; https://doi.org/10.4271/2000-01-2884 [CrossRef] [Google Scholar]

[43] Silverstein RM, Webster FX, Kiemle DJ. Spectrometric identification of organic compounds. 7th Ed. New Jersey: Jonh Wiley & Sons; 2005. [Google Scholar]

[44] Workman Jr, Weyer JL. Practical guide to interpretive near-infrared spectroscopy. 1st Ed. Boca Raton: CRC Press; 2008. [Google Scholar]

[45] Yang C, Yang Z, Zhang G, Hollebone B, Landriault M, Wang Z, Lambert P, Brown CE. Characterization and differentiation of chemical fingerprints of virgin and used lubricating oils for identification of contamination or adulteration sources. Fuel. 2016; https://doi.org/10.1016/j.fuel.2015.09.070 [CrossRef] [Google Scholar]

[46] Divya O, Mishra AK. Multivariate methods on the excitation emission matrix fluorescence spectroscopic data of diesel-kerosene mixtures: a comparative study. Anal Chim Acta. 2007; https://doi.org/10.1016/j.aca.2007.03.079 [CrossRef] [Google Scholar]

[47] Monograph NIR spectroscopy. A guide to near-infrared spectroscopic analysis of industrial manufacturing processes. In: Metrohm NIR Systems. 2017. http://www.mep.net.au/wpmep/wpcontent/uploads/2013/05/MEP_Monograph_NIRS_81085026EN.pdf. Accessed 29 Oct 2018. [CrossRef] [Google Scholar]